IOP Publishing Plasma Physics and Controlled Fusion

Plasma Phys. Control. Fusion 64 (2022) 045018 (9pp) https://doi.org/10.1088/1361-6587/ac4b05

Gyro-average method for global gyrokinetic particle simulation in realistic tokamak geometry

Yihao Duan[1], **Yong Xiao**[1,*] and **Zhihong Lin**[2]

[1] Institute for Fusion Theory and Simulation, Zhejiang University, Hangzhou, 310027, People's Republic of China

[2] Physics and Astronomy, University of California, Irvine, CA 92697, United States of America

E-mail: yxiao@zju.edu.cn

Received 7 October 2021, revised 19 December 2021
Accepted for publication 13 January 2022
Published 28 February 2022

Abstract

Gyro-average is a crucial operation to capturing the essential finite Larmor radius (FLR) effect in gyrokinetic simulation. In order to simulate strongly shaped plasmas, an innovative multi-point average method based on non-orthogonal coordinates has been developed to improve the accuracy of the original multi-point average method in gyrokinetic particle simulation. This new gyro-average method has been implemented in the gyrokinetic toroidal code (GTC). Benchmarks have been carried out to prove the accuracy of this new method. In the limit of concircular tokamak, ion temperature gradient (ITG) instability is accurately recovered for this new method and consistency is achieved. The new gyro-average method is also used to solve the gyrokinetic Poisson equation, and its correctness is confirmed in the long-wavelength limit for realistically shaped plasmas. The improved GTC code with the new gyro-average method is used to investigate the ITG instability with EAST magnetic geometry. The simulation results show that the correction induced by this new method in the linear growth rate is more significant for short-wavelength modes where the FLR effect becomes important. Due to its simplicity and accuracy, this new gyro-average method can find broader applications in simulating shaped plasmas in realistic tokamaks.

Keywords: gyrokinetic simulation, particle-in-cell, drift wave instability, verification and validation, gyro-average method, shaped plasmas

(Some figures may appear in colour only in the online journal)

1. Introduction

First-principles gyrokinetic simulation has been widely adopted to study low-frequency micro instabilities and turbulences in magnetic fusion plasmas [1, 2]. The gyro-average transformation, a frequent operation used in gyrokinetic simulation, is a procedure to average physical quantities such as electric potential and charge density along the cyclotron orbit [3–5]. To preserve the finite Larmor radius (FLR) effect, the gyro-average needs to be accurate enough to achieve high numerical fidelity. As one of the numerical algorithms for performing gyro-average, the multi-point average method has been developed and used extensively in gyrokinetic particle simulation [1, 6].

Simulations with realistic tokamak geometry, which is usually characterized by features such as up–down asymmetry and non-circularity, are crucial to interpret and predict various complicated tokamak experimental phenomena [7–9]. However, such geometric characteristics will lead to a large deviation from regular grid distribution and coordinate orthogonality. These deviations bring significant numerical challenges to the multi-point average method in gyrokinetic simulation.

[*] Author to whom any correspondence should be addressed.

In this article, an innovative multi-point method based on non-orthogonal magnetic coordinates has been developed and implemented in the global gyrokinetic toroidal code (GTC) [2]. This new method modifies the original multi-point average procedure in GTC to accommodate arbitrary magnetic geometry with sufficient concision and high accuracy, and captures more precisely the FLR effect that is important in computing linear eigenmodes and nonlinear turbulence [1]. Due to its simplicity and accuracy, the new method may be implemented in other gyrokinetic codes for simulating experimental plasmas.

Let us detail the physical quantities and equations involving gyro-average in the gyrokinetic particle simulation. Generally, two classes of equations involve this gyro-average procedure, namely the Maxwell equations to solve for self-consistent electromagnetic fields and equations of motion to push gyrocenter in phase space. To evolve the position and velocity of the gyrocenter, the gyro-averaged magnetic and electric fields are needed in the equations of motion, e.g. the gyro-averaged electrostatic potential $\bar{\phi}$ is defined as

$$\bar{\phi}(\boldsymbol{R}) = \frac{1}{2\pi}\int \phi(\boldsymbol{x})\delta(\boldsymbol{x}-\boldsymbol{R}-\boldsymbol{\rho})\mathrm{d}\boldsymbol{x}\mathrm{d}\varphi \tag{1}$$

where $\boldsymbol{R}$ is the gyrocenter position, $\boldsymbol{x}$ is the particle position, and φ stands for the gyrophase angle. The Larmor radius $\boldsymbol{\rho} \equiv -\mathbf{v}_\perp \times \hat{b}/\Omega$ with $\hat{b} \equiv \mathbf{B}/B$ and $\Omega \equiv qB/mc$. In the electrostatic limit, the Maxwell equations can be simplified to be the gyrokinetic Poisson equation, which is essentially the quasi-neutrality condition with the validity limit of $k_\perp^2\lambda_\mathrm{d}^2 \leqslant 1$ [6, 10, 11]:

$$\frac{\tau}{\lambda_\mathrm{d}^2}(\phi-\tilde{\phi}) = 4\pi e(\delta\bar{n}_\mathrm{i}-\delta n_\mathrm{e}), \tag{2}$$

where $\tau \equiv T_\mathrm{e}/T_\mathrm{i}$, $\lambda_\mathrm{d} \equiv \sqrt{T_\mathrm{e}/4\pi n_0 e^2}$ is the electron Debye length, n_0 is the equilibrium particle density, and the electrostatic potential ϕ is the unknown to be solved for. In equation (2), $\delta\bar{n}_\mathrm{i}$ and δn_e are the gyro-averaged ion and electron densities, respectively, with $\delta\bar{n}_\mathrm{i}$ defined as

$$\delta\bar{n}_\mathrm{i} = \frac{1}{2\pi n_0}\int \delta f_\mathrm{i}(\boldsymbol{R},\mu,v_\parallel)\delta(\boldsymbol{R}-\boldsymbol{x}+\boldsymbol{\rho})\mathrm{d}\boldsymbol{R}\mathrm{d}\mu\mathrm{d}v_\parallel\mathrm{d}\varphi, \tag{3}$$

where μ is the magnetic moment, $v_\parallel$ is the parallel velocity, and δf_i is the perturbed ion gyrocenter distribution. δn_e employs the same definition of equation (3) but δf_i is replaced by δf_e. Note that the electron gyro-radius is negligibly small and drift kinetics is usually assumed for the electron in the simulation. In equation (2), $\tilde{\phi}$ is the second gyro-averaged potential or double gyro-averaged potential, and is defined as

$$\tilde{\phi}(\boldsymbol{x}) = \frac{1}{2\pi}\int \bar{\phi}(\boldsymbol{R})F_\mathrm{M}(\boldsymbol{R},\mu,v_\parallel)\delta(\boldsymbol{R}-\boldsymbol{x}+\boldsymbol{\rho})\mathrm{d}\boldsymbol{R}\mathrm{d}\,\mu\mathrm{d}v_\parallel\mathrm{d}\varphi \tag{4}$$

where F_M is the Maxwellian distribution of the gyrocenter, and the gyro-averaged electric potential $\bar{\phi}(\boldsymbol{R})$ can be calculated by equation (1).

As discussed, the gyro-average transformation needs to be performed on the electromagnetic fields and charge density to push the gyrocenter in the phase space, and a second gyro-average transformation needs to be performed on the electrostatic potential to solve for the electromagnetic fields via the Poisson equation. Such gyro-averaged quantities can be calculated in the wavenumber ($\boldsymbol{k}$) space. However, the spectral method is most conveniently implemented in the flux-tube simulations, which drops off the background profile effects and is essentially a local approximation [6]. The multi-point average method (typically four-point) has been developed to evaluate the gyro-averaged quantities numerically, which is usually more advantageous in real space for global simulations [1, 6]. For the second gyro-average, there is another approach based on the Padé approximation [12], i.e. evaluating the second gyro-averaged potential $\tilde{\phi}$ by $\tilde{\phi} = \phi/(1-\rho_i^2\nabla_\perp^2)$. The Padé approximation can change the double integral operation of $\tilde{\phi}$ to be a second-order differential form and thus avoid the complicated multi-point average procedure, which can be used to solve the gyrokinetic Poisson equation for strongly shaped plasmas [9].

In practice, the multi-point average method could be more accurate than the Padé approximation for short wavelength modes with $k_\perp^2\rho_i^2 \geqslant 1$ [6]. However, the original multi-point method implemented in the GTC code is designed for orthogonal or weakly non-orthogonal coordinate systems [6]. It remains a bottleneck for the multi-point average method to accurately simulate strongly shaped plasmas.

In this paper, we present an innovative multi-point average method based on non-orthogonal magnetic coordinates, which can simulate arbitrarily shaped plasmas. This new method is implemented in the GTC code and then carefully benchmarked. The GTC simulation results show that the correction induced by this new method does make a difference on the ITG growth rates for the short wavelength modes where the FLR effect becomes important. The remainder of this paper is organized as follows. The necessity of finding a new gyro-average method for strongly shaped plasma is introduced in section 2. The scheme for the new multi-point gyro-average method is illustrated in section 3, then we present two examples to benchmark this new gyro-average method in section 4. The new gyro-average method is applied to study the ITG modes in section 5. Section 6 summarizes this paper and discusses possible future work.

2. Original four-point average method

In this section, we review the original four-point average method based on the magnetic coordinate that is implemented in the GTC code.

The magnetic flux coordinates have been widely used for describing the equilibrium magnetic field of toroidal confinement systems [13] in gyrokinetic simulations. A particular set of magnetic flux coordinates, namely the Boozer coordinates (ψ,θ,ζ) [14], is chosen in the GTC code to push particles and solve for electromagnetic fields, where ψ is the poloidal flux

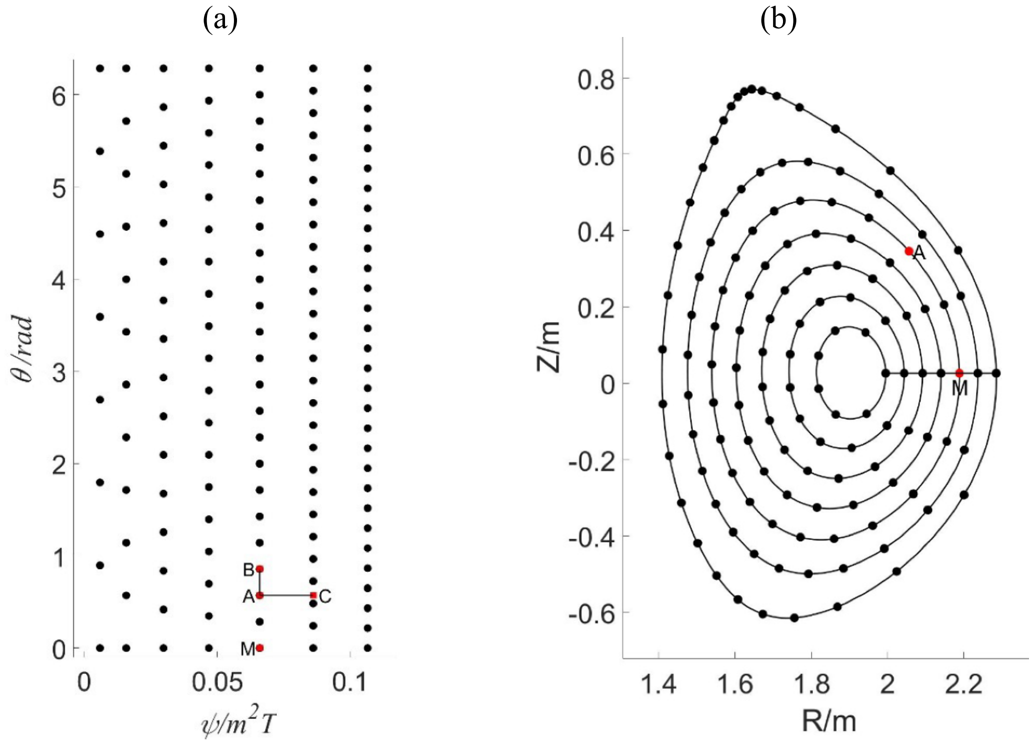

Figure 1. Example of mesh grid distribution on (a) the (ψ,θ) plane and (b) the (R,Z) plane for typical EAST shaped plasmas (Shot # 077741.03500).

or radial-like variable, θ is the poloidal angle, and ζ is the toroidal angle. With the Boozer coordinates, we can conveniently define a field-aligned mesh that captures the essential flute mode structure of turbulence with $k_{\parallel} \ll k_{\perp}$ and requires only a few dozens of toroidal grids to accelerate field calculation by a factor varying from several tens to hundreds [9].

The next two approximations have been employed in GTC code without losing accuracy and greatly facilitate the numerical implementation of the four-point average procedure for large aspect ratio tokamaks. First, the toroidal angle in the Boozer coordinates ζ is approximated to the toroidal angle in the cylindrical coordinates (R,ϕ_{t},Z) with $\zeta \approx -\phi_{\mathrm{t}}$, since the difference function $\nu(\psi,\theta) \equiv \zeta + \phi_{\mathrm{t}}$ turns out to be of order $O\left(\varepsilon^2\right)$ for tokamaks with the inverse aspect ratio $\varepsilon = r/R_0 \ll 1$. Next, the perpendicular plane is approximated to the poloidal plane, since the intersection angle δ between them is second-order small in ε, i.e. $\delta\sim \mathrm{O}\left(\varepsilon^2/q^2\right)$, which comes from evaluating $\cos\delta = \mathbf{B}\cdot\nabla\zeta/B|\nabla\zeta|$. For example, it is evaluated numerically that the intersection angle δ is no more than 0.089 for the typical EAST equilibrium, as is shown in section 5.

The original four-point average method has been widely used and well benchmarked for weakly shaped plasma [6, 9]. However, the strong shaping of the magnetic flux could lead to significant deviation against the implicit assumption in the original four-point scheme. Here, we illustrate this deviation and necessity for improvement using a single-null-divertor equilibrium configuration of the EAST tokamak (Shot # 077741.03500). Figure 1 shows GTC's field mesh setting on the toroidal plane with $\zeta = 0$. The GTC code uses evenly spaced radial grids at $\theta = 0$, as is shown by the black straight line in figure 1(b). In the poloidal direction, the grid size $\Delta\theta$ is uniform on each flux surface while maintaining $r\Delta\theta \sim \Delta r$, as is shown in figure 1(b). The corresponding grid setting on the (ψ,θ) plane is shown in figure 1(a). The relatively regular grid distribution on the (ψ,θ) plane offers great convenience for numerical operations such as field interpolation and particle deposition.

To illustrate the original four-point average method, we consider one particular field point A with the coordinates (ψ,θ) in figure 1 as the gyrocenter position for gyro-average. In figure 1(a), point B is the poloidal grid next to the field point A along constant ψ, and Point C is the intersection point on the next flux surface along constant θ. In the original method, the four points selected for gyro-average are located at $(\psi\pm\delta\psi,\theta)$ and $(\psi,\theta\pm\delta\theta)$, which are supposed to center at (ψ,θ) with a radius ρ_i. The difference $\delta\psi$ and $\delta\theta$ are calculated by the following relationship:

$$\delta\psi = \frac{\rho_i}{l_{AC}}\psi_{AC},\ \delta\theta = \frac{\rho_i}{l_{AB}}\theta_{AB} \tag{5}$$

where $\psi_{AC} = \psi_C - \psi_A$, $\theta_{AB} = \theta_B - \theta_A$. Using the constructed B-splines in GTC [9], the (R,Z) coordinates can be calculated for the selected four points. l_{AC} and l_{AB} can be calculated by $\sqrt{(R_A-R_C)^2+(Z_A-Z_C)^2}$ and $\sqrt{(R_A-R_B)^2+(Z_A-Z_B)^2}$, respectively.

After calculating $\delta\psi$ and $\delta\theta$, we present the selected four points $(\psi\pm\delta\psi,\theta)$ $(\psi,\theta\pm\delta\theta)$ in figure 2 by four red square markers. It can be seen that these four squares are close to

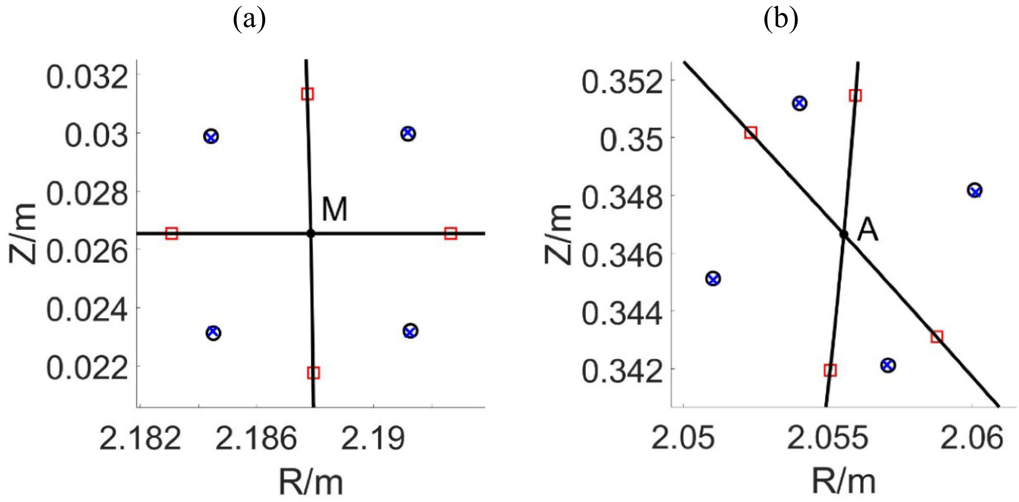

Figure 2. Demonstration of the four-point average at the field grid point A: the black circles are the exact points in the four-point average method, the red squares are from the original gyro-average method, and the blue crosses are produced by the improved gyro-average method. The two solid lines are the contour lines for constants ψ and θ, respectively.

equally spaced points on the circle centered about the field point M, as is shown in figure 2(a), but they are far away from equally spaced points on the circle centered about the field position A, as shown in figure 2(b). To figure out why this inaccuracy arises, we draw two contour lines with constants ψ and θ, respectively. These two lines intersect at the points M and A, respectively, as is shown by figures 2(a) and (b). The constant ψ line is almost orthogonal to the constant θ line in figure 2(a) but far away from the orthogonal in figure 2(b). It is the non-orthogonality of the Boozer coordinate (ψ, θ), or the non-orthogonality of $\nabla\psi$ and $\nabla\theta$, that causes the uneven distribution of the selected four points on the gyro-average circle. We have tested various field points in the whole poloidal plane and found that the selected four points are much more inaccurate for gyro-average in the plasma edge than that in the plasma core, since the non-orthogonality of the Boozer coordinates are more severe in the plasma edge.

To quantify how much inaccuracy the original four-point method can bring by the coordinate non-orthogonality, we define α as the intersection angle between $\nabla\psi$ and $\nabla\theta$, ranging from 0 to π, and α can be calculated by

$$\cos\alpha = \frac{\nabla\psi\cdot\nabla\theta}{|\nabla\psi|\,|\nabla\theta|}. \tag{6}$$

Then we show the intersection angle α in the 2D contour plot of figure 3. As can be seen, the angle α is exactly equal to $\pi/2$ at $\theta = 0$ where the point M is located. About 45% of the whole area has a moderate angle deviation (less than 30%) from $\pi/2$. The derivation is more severe in those areas close to the plasma edge, as is shown by figure 3. In some edge areas, the deviation could be even larger than 60%.

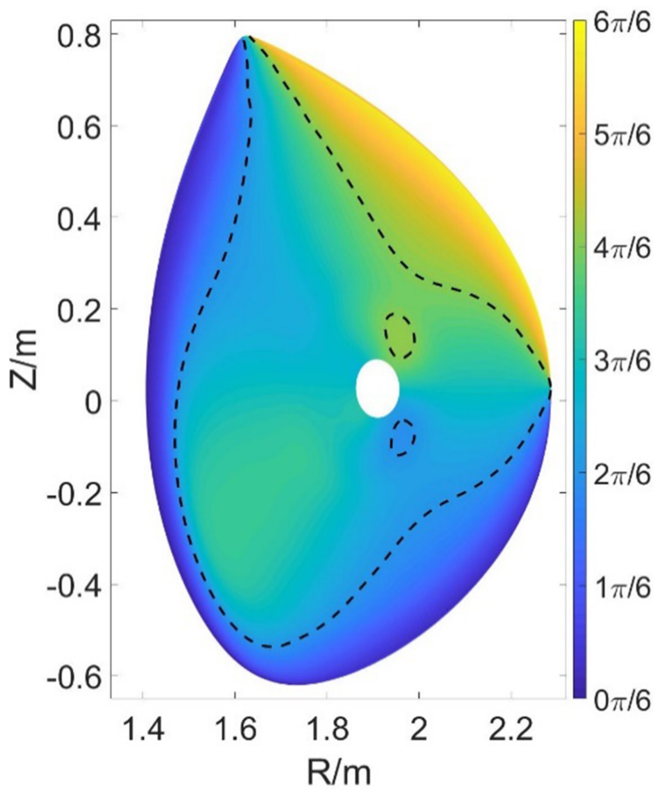

Figure 3. Contour plot for the intersection angle α on the poloidal plane with the contour lines at $\alpha = 2\pi/6$ and $\alpha = 4\pi/6$ shown by the dashed black lines.

3. Improved gyro-average for shaped plasmas

A new numerical method is highly in demand to accommodate this coordinate non-orthogonality for the strongly shaped plasmas. The key idea of this new method is to locate the accurate positions for the gyro-average points by including the non-orthogonality between the radial and poloidal coordinates. The positions of these gyro-average points produced by the new method are given by $(\psi + \Delta\psi_j, \theta + \Delta\theta_j)$, with

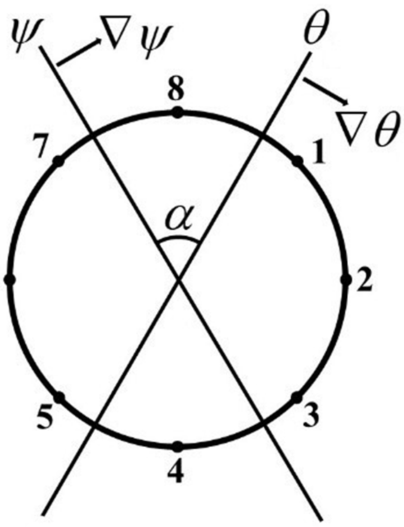

Figure 4. Illustration of the improved gyro-average method based on non-orthogonal coordinates.

$$\Delta\psi_j = \sin\left(\frac{2\pi j}{N} + \frac{\alpha}{2}\right)\frac{\delta\psi}{\sin(\alpha)},$$
$$\Delta\theta_j = \sin\left(\frac{2\pi j}{N} - \frac{\alpha}{2}\right)\frac{\delta\theta}{\sin(\alpha)}, \ (j = 1, 2, \ldots, N), \quad (7)$$

where the intersection angle α is given in equation (6), and $\delta\psi$ and $\delta\theta$ are defined by equation (5). N could be 4, 8, etc, corresponding to the number of points used for the gyro-average. Assuming that $N = 8$, the schematic diagram for this new eight-point average method is shown in figure 4. Two contour lines for constants ψ and θ are shown by the two black solid lines. The vectors $\nabla\psi$ and $\nabla\theta$ are marked in figure 4, which are perpendicular to their contour lines, respectively. As is shown in figure 4, the new method produces eight points systematically by $(\psi + \Delta\psi_j, \theta + \Delta\theta_j), j = 1, 2 \ldots 8$.

The four-point or sixteen-point average can be produced by the same strategy. For example, we can select four points from the eight points in figure 4, namely the points with index j = 2, 4, 6, 8, to carry out the four-point average procedure, as is shown in figure 2 by the blue crosses. By comparison, we also show the exact points by a brutal force calculation in figure 2 using black circles. It can be seen that the selected four points from the improved gyro-average method well match the exact four points. To verify the accuracy and generality of the new method, we tested various field points in different equilibrium magnetic configurations, such as China Fusion Engineering Test Reactor. The correction effect of the new method is similar to that presented in figure 2.

One may argue that the contour lines for constants ψ and θ may not be straight lines within the range of one gyro-orbit and thus numerical inaccuracy could arise. However, for typical fusion plasmas, the ratio between gyro-radius and the curvature radius of the field line is of the order $O(\rho_i/R_0)$. Thus, this new method can be used to improve the original gyro-average operation in GTC with satisfactory accuracy. In addition, this improved gyro-average method possesses a number of highly desirable features such as systematic treatment of points and minimal modifications to the original GTC code, which make this new method appealing not only to GTC but also to other gyrokinetic codes.

4. Benchmarks for improved gyro-average method

In this section, we implement the improved gyro-average method in the GTC code and verify its effectiveness with two examples. First of all, the improved four-point method should conform with the original four-point average method in the limit of concentric circular tokamak where the original procedure is still accurate. Secondly, it is crucial to verify the accuracy of the improved four-point method by solving the classical Poisson problem $-\nabla_\perp^2\phi = \delta n$ correctly with realistic geometry.

4.1. Consistency check: concentric circular geometry

For the concentric circular magnetic field, the magnetic surface is determined by the equations

$$R = R_0 + r\cos\theta_g \quad (8)$$

$$Z = r\sin\theta_g. \quad (9)$$

The Boozer coordinates (ψ, θ, ζ) are constructed analytically as follows: the poloidal magnetic flux ψ can be determined by $\mathrm{d}\psi_\mathrm{t}/\mathrm{d}\psi = q(\psi)$ with the toroidal magnetic flux $\psi_\mathrm{t} = r^2/2$. The Boozer poloidal angle θ can be determined by $\theta = \theta_g - r\sin\theta_g$, and the Boozer toroidal angle ζ can be determined by $\zeta = -\phi_\mathrm{t}$. Now we can calculate the intersection angle α in equation (6). This angle turns out to be not far away from $\pi/2$, with a deviation of less than 5% in most areas and a maximum value of 17% for the large aspect ratio tokamak with $r/R < 0.3$. As we have discussed in section 2, the main inaccuracy for the original four-point average method comes from the non-orthogonality between $\nabla\psi$ and $\nabla\theta$. Since the non-orthogonality is weak in this case, the inaccuracy is insignificant according to our analysis. Therefore, the improved four-point average method should conform with the original scheme.

To confirm our conjecture, we use the Cyclone Base parameters in [15] to carry out a global gyrokinetic simulation via the GTC code for ion temperature gradient (ITG) instability, with the concentric circular geometry defined in equations (8) and (9) for the equilibrium magnetic field. The background temperature and density are set as $T_\mathrm{e} = T_\mathrm{i} = 2.223\,\mathrm{keV}$ and $n_\mathrm{i} = n_\mathrm{e} = 7.9 \times 10^{19}\ \mathrm{m}^{-3}$, respectively. The inverse aspect ratio is set as $a/R_0 = 0.36$ with the major radius $R_0 = 0.835\ m$, and the simulation domain is set as $r \subset [0.1a, 0.9a]$. At $r = a/2$ flux surface, we have the following local simulation parameters: $r/R_0 = 0.18$, safety factor $q = 1.4$, magnetic shear $s = q'r/q = 0.78$, density gradient $R_0/L_n = 2.22$, and ion or electron temperature gradient $R_0/L_T = 6.92$, where L_T and L_n are the temperature and density gradient scale lengths, defined by $L_T \equiv -(\mathrm{d}\ln T/\mathrm{d}r)^{-1}$ and $L_n \equiv -(\mathrm{d}\ln n/\mathrm{d}r)^{-1}$. Here, we focus on the ion physics and plasma-shaping effect, and the electrons are assumed to be adiabatic for simplicity.

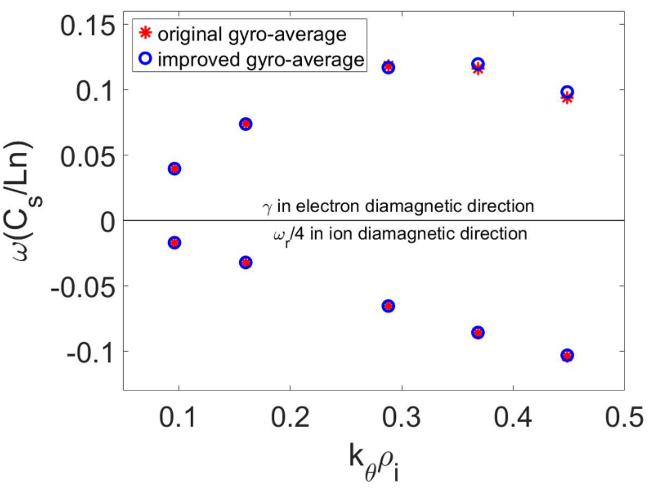

Figure 5. Linear growth rate γ and real frequency $\boldsymbol{\omega_r}$ of ITG as functions of the poloidal wavenumber in the concentric circular tokamak.

The linear simulation results on the ITG dispersion are demonstrated in figure 5. The linear dispersion relation from this improved gyro-average method matches that from the original gyro-average method in both growth rate and real frequency, with a difference of less than 5%. Thus, we confirm that the improved gyro-average method is consistent with the original gyro-average method in the limit of the concentric circular tokamak, as it should be.

4.2. Gyrokinetic Poisson solver: EAST magnetic geometry

Next, we come to solve the gyrokinetic Poisson equation (equation (2)) in the long-wavelength limit with a typically shaped plasma equilibrium from the EAST tokamak experiments. Note that the gyrokinetic Poisson equation becomes two-dimensional in the limit of $k_\parallel \ll k_\perp$ and becomes the standard Poisson problem $-\rho_i{}^2 en_0\nabla_\perp^2\phi = T_i\delta n$ since the approximation $\phi - \tilde{\phi} \approx -\rho_i^2\nabla_\perp^2\phi$ holds in the long-wavelength limit.

Various benchmarks [6, 9] on the four-point average method have been carried out in the large aspect ratio circular cross-section limit since the Poisson problem is essentially a Bessel problem in this limit and its solutions are known analytically. However, such experience cannot be easily applied to the realistically shaped geometry where the new method is expected to make a notable difference. A new numerical scheme has been designed to verify the accuracy of the Poisson solver with improved four-point average by the following procedure: (a) Given a known analytic function expression $F(\psi,\theta)$; (b) calculate the charge density δn numerically by $\delta n \equiv -\nabla_\perp^2 F$; (c) use the resulting δn as the source to the Poisson equation and solve the Poisson equation $-\nabla_\perp^2\phi = \delta n$ by employing the four-point average method; (d) compare the calculated ϕ with the original function $F(\psi,\theta)$ and compute the error by their difference. If $F \approx \phi$ or the error is sufficiently small, we can conclude that this four-point average method is sufficiently accurate. As can be seen, an analytical solution can be conveniently established in the long wavelength, but not in the short wavelength, because the calculation of charge density cannot be simplified to the form in step (b).

In this benchmark case, the aforementioned EAST equilibrium is used for the shaped plasma. The specific benchmark function is given by: $F(\psi,\theta) = (\psi-\psi_0)^3(\psi_1-\psi)^3\cos(m\theta)$ with $m = 6$, where $\psi_0 = \psi(r = 0.55a)$ and $\psi_1 = \psi(r = 0.95a)$ are the poloidal flux at the inner and outer boundaries, respectively.

The resulting charge density δn is shown in figure 6(a). The prescribed function $F(\psi,\theta)$ is shown in figure 6(b), which is also the analytic solution of the Poisson equation $-\nabla_\perp^2\phi = \delta n$. As can be seen, the difference between δn and $F(\psi,\theta)$ is significant. The numerical solution to the Poisson equation is demonstrated in figure 7(c) where the original four-point average method is used, and in figure 7(d), where the improved four-point average method is used. The numerical solution in figure 7(d) is almost identical to the analytical solution in figure 7(b), which proves the accuracy of the improved four-point average method. However, the numerical solution in figure 7(c) differs from the analytical solution in figure 7(b), and its 2D pattern is more like that of the source term δn in figure 7(a).

For a more quantitative comparison, we take out the data along the black solid line in figures 6(b)–(d), then compare them in a one-dimensional plot in figure 7, where the black line represents the analytical solution F, the blue circle stands for the numerical solution using the improved four-point average method, and the dashed red line represents the numerical solution using the original four-point average method. As can be seen in figure 7, there is a notable difference between the red dashed line and the black solid line, especially on the left or center of the figure. We further note that this difference exists not only on this particular line but also on the whole poloidal plane, which suggests that the original four-point average needs to be improved for better accuracy. However, the difference is almost indistinguishable between the blue circles and black solid lines, which verifies the high accuracy of the improved four-point average method. By scanning the whole poloidal plane, we find that the numerical solution using the improved four-point method matches the exact analytic solution very closely. The slight difference between them comes from the difference in numerical operator. The operator for the four-point average method in this benchmark is $0.7194J_0^2(0.9130k_\perp\rho_i) + 0.2806J_0^2(2.2339k_\perp\rho_i) - 1$, and the exact operator we wanted is $(k_\perp\rho_i)^2$. In the long wavelength limit $k_\perp\rho_i \to 0$, the two operators can be considered the same. However, there is always a difference between these two operators when $k_\perp\rho_i$ is finite, albeit it is small when $k_\perp\rho_i$ is small.

Combining both benchmarks in this section and the verification in section 3, we conclude that the improved four-point average method can be utilized to significantly improve the gyro-average procedure to obtain an accurate gyro-averaged potential as well as ion density, which is crucial for the PIC simulation to simulate shaped plasmas because the inaccuracy in the gyro-average can accumulate at each time step and may substantially modify the linear and nonlinear simulation results.

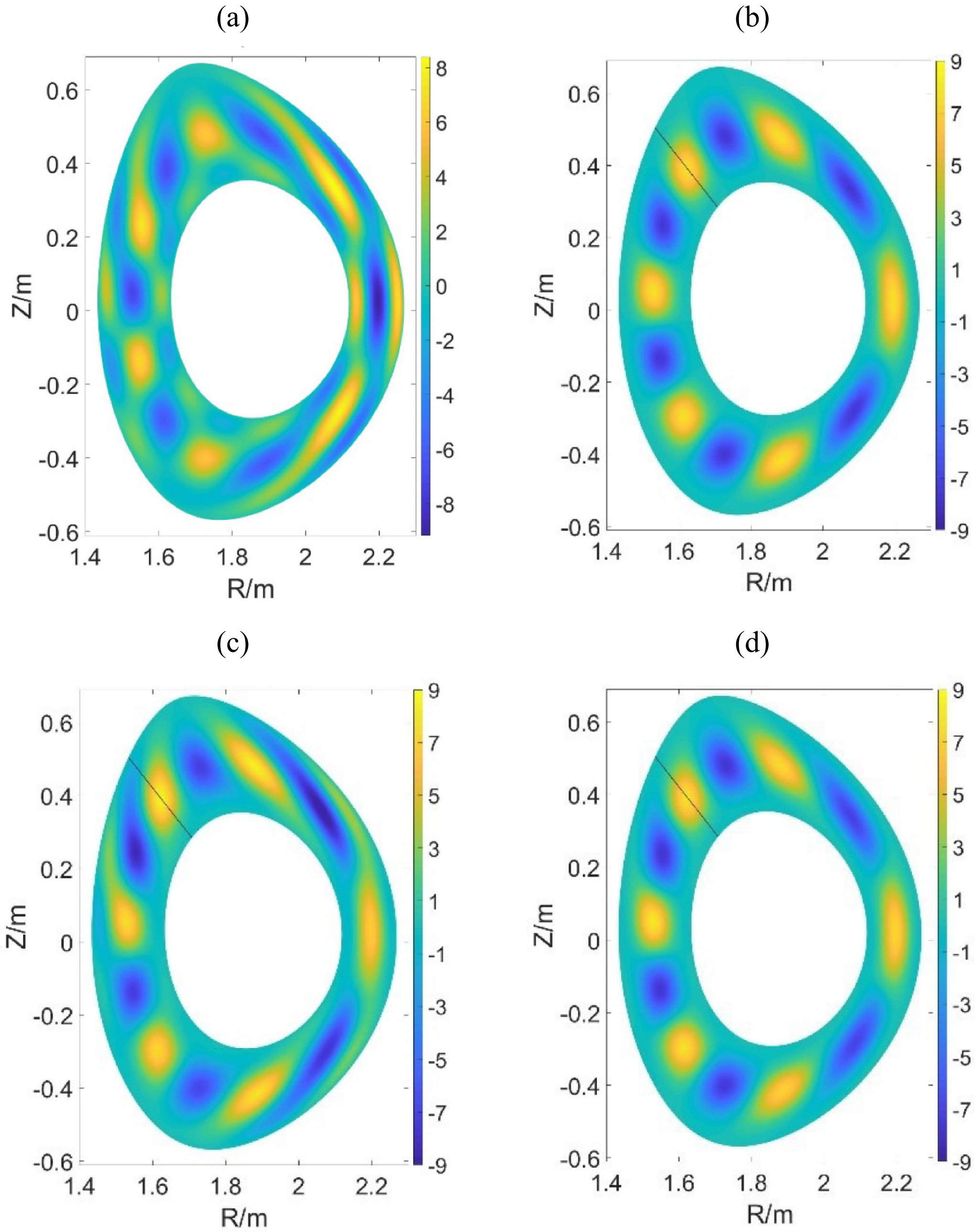

Figure 6. (a) Density fluctuation δn on poloidal plane. (b) Given analytic function F on poloidal plane. (c) Numerical solution ϕ from original four-average method. (d) Numerical solution from improved four-average method.

5. ITG mode for EAST geometry

In this section, we carry out the ITG simulation with adiabatic electrons using the aforementioned EAST equilibrium (shot# 077741.03500). The equilibrium data, such as poloidal flux $\psi(R,Z)$, poloidal current I, and safety factor q have been used to construct the equilibrium magnetic field in real space and determine the Boozer coordinates (ψ,θ,ζ). This shaped EAST equilibrium has a background magnetic field with up–down asymmetry and the tokamak parameters $B_0 = 2.46\,\mathrm{T}$, $a = 0.375m$, $R_0 = 1.91m$. On the reference flux surface at the middle of the minor radius, $T_\mathrm{i} = T_\mathrm{e} = 1500\,\mathrm{keV}$ and $n = 4.0\times10^{19}\,\mathrm{m}^{-3}$. For simplicity, we choose the Cyclone base case parameters $R_0/L_n = 2.22$, $R_0/L_T = 6.92$ for the plasma gradients.

The intersection angle between the Boozer coordinates ψ and θ has been computed in figure 3, and the moderate coordinate non-orthogonality suggests that the improved gyro-average method can play an important role according to the preceding discussions.

The gyro-average procedure is associated with the FLR effect, an essential kinetic effect in magnetized plasmas. The more accurate we treat the gyro-average, the more accurate we calculate the FLR effect. It is known that the FLR effect plays an important role in determining the ITG growth rate, especially for higher n modes [16]. Therefore, we expect that

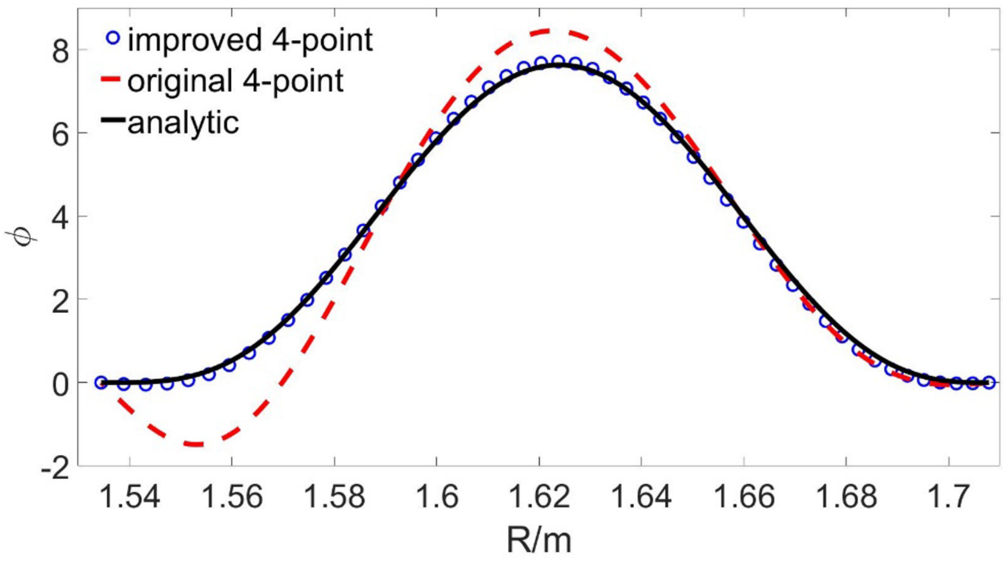

Figure 7. Comparison of solutions along the black line in figure 6.

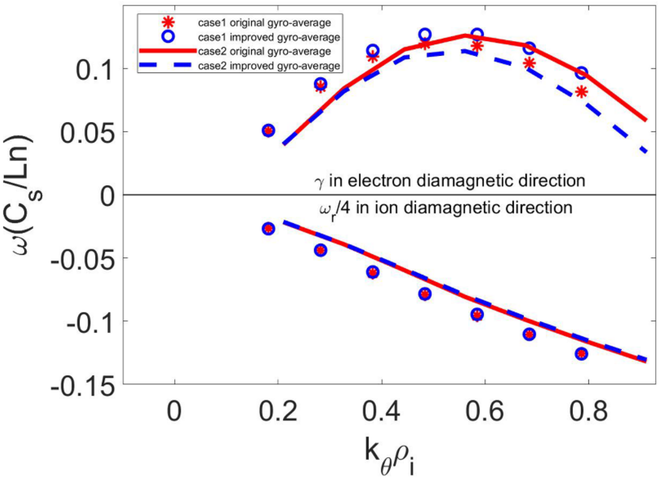

Figure 8. The linear growth rate γ and real frequency $\boldsymbol{\omega}_{\mathbf{r}}$ of ITG as functions of the poloidal wavenumber in EAST tokamak.

with the application of the improved gyro-average method, the correction to the gyro-average procedure can make significant changes for the ITG growth rates, especially for those high n modes.

The GTC linear ITG simulation results are shown in figure 8, where the linear growth rate and frequency vary with poloidal wavelength $k_\theta \rho_i$. In this figure, the blue color represents simulation results using the improved four-point average method, while the red color represents simulation results using the original four-point average method; case 1 and case 2 represent two different radial domains used in the simulation. As discovered in section 2, the coordinate non-orthogonality varies in the poloidal plane. In order to demonstrate its consequence on the linear instability, we artificially set the radial simulation domain: $r \subset [0.55a, 0.95a]$ for case 1, and $r \subset [0.30a, 0.70a]$ for case 2.

As can be seen in figure 8, for either case 1 or case 2, the linear growth rate using the improved four-point average converges to that using the original four-point average in the long-wavelength limit. With the poloidal wavenumber increasing, the FLR effect becomes more important, and the difference for linear growth rate between the two gyro-average methods becomes larger. This trend is demonstrated in figure 8 as well. The difference for real frequency is mainly determined by the diamagnetic frequency ω_*, which does not contain the FLR effect. That is why the real frequency is indistinguishable between different gyro-average methods. However, the real frequency for case 1 (outer radial domain) is generally larger than that for case 2 (inner radial domain). This is due to the fact that the average magnetic field for case 1 is smaller than that for case 2 and thus the corresponding diamagnetic frequency is larger for case 1 when the most unstable area outside the middle plane is considered.

6. Conclusion

In this paper, we have found the main source of inaccuracy introduced by the original gyrophase-average procedure in a realistic tokamak geometry, i.e. the non-orthogonality of the Boozer coordinates [6, 9], and developed an innovative multi-point average method to improve the computing accuracy. The effectiveness and accuracy of this new method is demonstrated by a number of benchmark cases such as consistency check and solving the gyrokinetic Poisson equation. For the conventional ITG instability case, we find that the improved four-point average method calculates the FLR effect more accurately, demonstrated by the difference of the linear growth rates in the short-wavelength range between this new four-point average method and the original one. Based on the improved multi-point average method, we plan to simulate turbulence physics in spherical tokamak and the edge of tokamak, where this new method can find broader applications for its usefulness. In addition, the current work is focused on electrostatic turbulence simulation. The electromagnetic gyrokinetic simulation for shaped plasmas is another interesting direction to explore with this new gyro-average method.

Data availability statement

The data that support the findings of this study are available upon reasonable request from the authors.

Acknowledgments

This work is supported by National MCF Energy R & D Program of China Nos. 2019YFE03060000 and 2015GB110000, and by NSFC under Grant No. 11975201.

ORCID iD

Yong Xiao https://orcid.org/0000-0001-5333-2867

References

[1] Lee W W 1987 *J. Comput. Phys.* **72** 243
[2] Lin Z, Hahm T S, Lee W W, Tang W M and White R 1998 *Science* **281** 1835
[3] Catto P J 1981 Generalized gyrokinetics *Plasma Phys.* **23** 639
[4] Frieman E A and Chen L 1982 *Phys. Fluids* **25** 502
[5] Hahm T S 1988 *Phys. Fluids* **31** 2670
[6] Lin Z and Lee W W 1995 *Phys. Rev.* E **52** 5646
[7] Lei Q, Kwon J, Hahm T S and Jo G 2016 *Phys. Plasmas* **23** 062513
[8] Wang W X, Lin Z, Tang W M, Lee W W, Ethier S, Lewandowski J L V, Rewoldt G, Hahm T S and Manickam J 2006 *Phys. Plasmas* **13** 092505
[9] Xiao Y, Holod I, Wang Z, Lin Z and Zhang T 2015 *Phys. Plasmas* **22** 022516
[10] Dubin D H E, Krommes J A, Oberman C and Lee W W 1983 *Phys. Fluids* **26** 3524
[11] Lee W W 1983 *Phys. Fluids* **26** 556
[12] LeBrun M J and Tajima T 1994 *Bull. Am. Phys. Soc.* **39** 1533
[13] D'Haeseleer W D, Hitchon W N and Callen J D 1991 *Flux Coordinates and Magnetic Field Structure* (Berlin: Springer)
[14] White R B 2006 *The Theory of Toroidally Confined Plasmas* 2nd edn (London: World Scientific Imperial College Press) Revised
[15] Dimits A M *et al* 2000 *Phys. Plasmas* **7** 969
[16] Hirose A 1985 *Phys. Rev. Lett.* **55** 5